Magnetic Radial Vortex Stabilization and Efficient Manipulation Driven by the Dzyaloshinskii-Moriya Interaction and Spin-Transfer Torque

G. Siracusano,[1] R. Tomasello,[2] A. Giordano,[1] V. Puliafito,[3] B. Azzerboni,[3] O. Ozatay,[4] M. Carpentieri,[5] and G. Finocchio[1,*]

[1]*Department of Mathematical and Computer Sciences, Physical Sciences and Earth Sciences, University of Messina, I-98166 Messina, Italy*

[2]*Department of Engineering, Polo Scientifico Didattico di Terni, University of Perugia, I-50100 Terni, Italy*

[3]*Department of Engineering, University of Messina, I-98166 Messina, Italy*

[4]*Department of Physics, Bogazici University, 34342 Bebek/Istanbul, Turkey*

[5]*Department of Electrical and Information Engineering, Politecnico di Bari, via E. Orabona 4, I-70125 Bari, Italy*

(Received 4 February 2016; revised manuscript received 20 May 2016; published 17 August 2016)

Solitons are very promising for the design of the next generation of ultralow power devices for storage and computation. The key ingredient to achieving this goal is the fundamental understanding of their stabilization and manipulation. Here, we show how the interfacial Dzyaloshinskii-Moriya Interaction (IDMI) is able to lift the energy degeneracy of a magnetic vortex state by stabilizing a topological soliton with radial chirality, hereafter called radial vortex. It has a noninteger Skyrmion number S ($0.5 < |S| < 1$) due to both the vortex core polarity and the magnetization tilting induced by the IDMI boundary conditions. Micromagnetic simulations predict that a magnetoresistive memory based on the radial vortex state in both free and polarizer layers can be efficiently switched by a threshold current density smaller than 10^6 A/cm^2. The switching processes occur via the nucleation of topologically connected vortices and vortex-antivortex pairs, followed by spin-wave emissions due to vortex-antivortex annihilations.

DOI: 10.1103/PhysRevLett.117.087204

Magnetic solitons, such as domain walls (DWs) [1–4], vortices [5–11], and Skyrmions [12–17], are attracting a growing interest for their potential technological applications in ultralow power devices beyond CMOS, thanks to their fundamental properties and the possible use of spin-transfer [18] and spin-orbit [2–4] torques for their nucleation and manipulation. For example, DWs and Skyrmions are at the basis of racetrack memories [3,4,12,19], while vortices can be used as an alternative to the uniform state to store information in magnetoresistive devices [5,11], such as magnetic tunnel junctions (MTJs). Furthermore, the presence of the additional degree of freedom of the exchangelike interfacial Dzyaloshinskii-Moriya Interaction (IDMI) [20] in the energy landscape of ferromagnetic materials has given rise to the possibility to speed up DW motion in racetrack memories [3,4], and stabilize Skyrmions in ultrathin ferromagnets [12,16]. While numerous theoretical and experimental studies have concentrated on the effect of the IDMI on the static and dynamical characterization of DWs [3] and Skyrmions [12,14,19], the understanding of its effect on vortices is still missing. In the absence of IDMI, vortices are characterized by polarity and chirality. The former indicates the direction of the vortex core, $+1$ or -1 if the core points along the positive or negative out-of-plane direction. The latter is linked to the orientation of the in-plane magnetization around the core. In this Letter, we show that a large enough IDMI can stabilize a vortex state characterized by a radial chirality [21], hereafter called *radial vortex*, where the in-plane components of the magnetization point radially from the vortex core to the boundary (outward) or *vice versa* (inward), depending on vortex polarity and IDMI sign. Figure 1 shows the spatial distribution of the magnetization for different types of vortex. The chirality can be counterclockwise (CCW), clockwise (CW), and radial. Here, we use the term *circular vortex* to identify a vortex with CW or CCW chirality. For a fixed polarity, in a circular vortex, both CCW and CW configurations are energetically equivalent (degeneracy in the energy landscape) [9]. On the

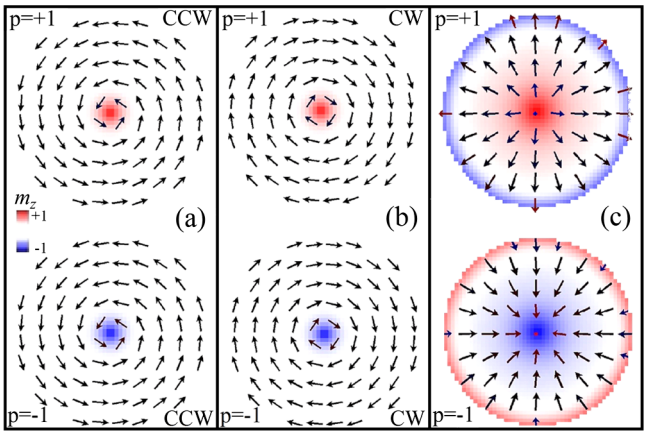

FIG. 1. Spatial distribution of magnetization for different types of vortex with positive (top) and negative (bottom) polarity. (a) Counterclockwise (CCW) circular vortex. (b) Clockwise (CW) circular vortex. (c) Radial vortex. A color scale linked to the out-of-plane component of the magnetization is also shown (red positive, blue negative).

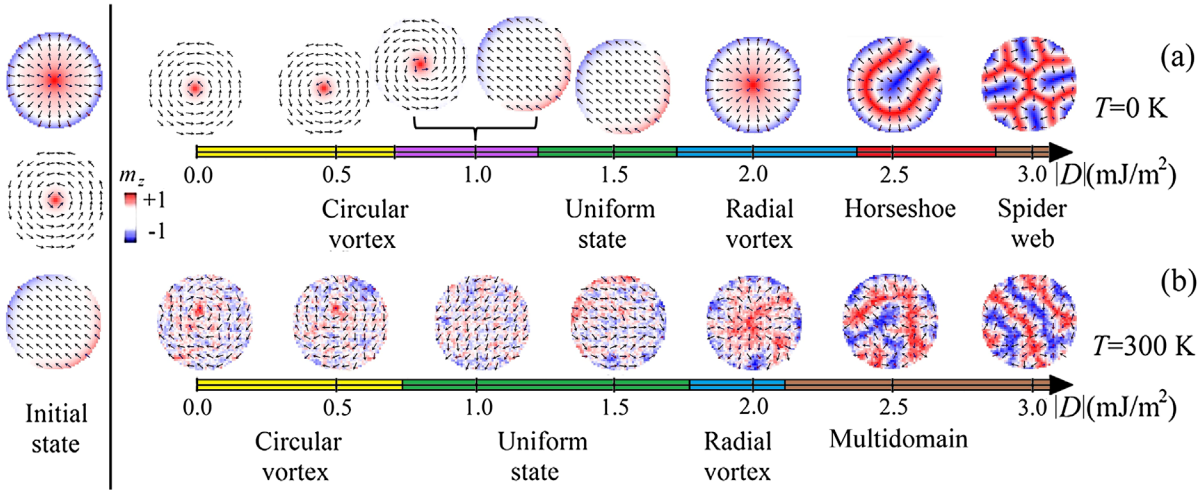

FIG. 2. Equilibrium configurations of the magnetization as a function of $|D|$ at zero external field when (a) $T = 0$ K and (b) $T = 300$ K. The snapshots are calculated for $|D| = 0.0$, 0.5, 1.0, 1.5, 2.0, 2.5, and 3.0 mJ/m^2. For $|D| = 1.0$ mJ/m^2 in (a), the two represented magnetization configurations depend on the initial state. The colors refer to the z component of the magnetization (blue negative, red positive). Left inset: the initial state can be radial or circular vortex, as well as the uniform state.

other hand, for a radial vortex, the core polarity fixes the chirality (radial and antiradial for positive or negative vortex core polarity, respectively), because of the nonsymmetric IDMI field. In other words, a large-enough IDMI removes the energy degeneracy of a vortex state.

From a fundamental point of view, the stabilization of a radial vortex gives rise to the possibility to create current densities with radial polarization for particle-trapping applications, such as Skyrmion [22], analogously to what radially polarized beams can do in many optical systems [23].

In order to show the main features and the possible applications of the radial vortex, extensive micromagnetic simulations have been performed. The first part of this Letter focuses on the fundamental properties of the radial vortex, in terms of stability as a function of the IDMI, topology, nucleation, as well as response to an in-plane field. The second part is dedicated to the analysis of the switching process of the radial vortex, underlining the differences with the circular vortex.

We consider a CoFeB disk having a diameter $d = 250$ nm and a thickness $t = 1.0$ nm to have an in-plane easy axis at zero external field. To add the IDMI, we consider the CoFeB coupled with a Pt (heavy metal) layer as already experimentally observed [24]. The study is carried out by means of a *state-of-the-art* micromagnetic solver which numerically integrates the Landau-Lifshitz-Gilbert equation [25–27], that includes the IDMI contribution $\mathbf{h}_{\mathrm{IDMI}}$ [28–30]. Here, we show results achieved for different values of the negative IDMI parameter D (in the rest of the Letter we indicate always the magnitude $|D|$ of the IDMI parameter), but both qualitatively and quantitatively similar results have been obtained for positive D with the difference that the radial chirality is reversed for a fixed polarity.

Stability.—The magnetization stability has been studied as a function of $|D|$ from 0.0 to 3.0 mJ/m^2 with a resolution of 0.1 mJ/m^2. For each $|D|$, we have performed simulations for three different initial magnetization configurations (uniform state, radial, and circular vortex). Figure 2(a) summarizes the final states achieved without thermal effects. Those magnetization patterns are independent of the initial state except in the range $0.7 < |D| < 1.2$ mJ/m^2, where both uniform state and circular vortex are *minima*. Figure 3 shows the Skyrmion number S as a function of the IDMI as computed from the topological density $S = (1/4\pi)\int \mathbf{m}\cdot(\partial_x \mathbf{m} \times \partial_y \mathbf{m})dxdy$ [41]. At low IDMI ($0.0 < |D| < 1.1$ mJ/m^2), S slightly increases from the zero IDMI case ($|S| = 0.5$) because of the IDMI boundary conditions. As $|D|$ increases, the uniform state is stable in the region $0.7 < |D| < 1.6$ mJ/m^2 ($|S| \approx 0$), while the radial vortex, characterized by $0.8 < |S| < 0.9$, is the final state in the range $1.7 < |D| < 2.3$ mJ/m^2. This stability diagram can be qualitatively understood as follows. For in-plane materials the effect of the IDMI can be seen as an additional shape anisotropy contribution [24]; thus, the different magnetic states [Fig. 2(a)] can be linked to a trade-off among magnetostatic, exchange, and IDMI energies. In particular, at low $|D|$, the magnetostatic energy is predominant, stabilizing a vortex with a circular chirality. Increasing $|D|$, the exchange ($0.7 < |D| < 1.6$ mJ/m^2) and the IDMI ($1.7 < |D| < 2.3$ mJ/m^2) energies become the main contributions, leading to uniform and radial vortex states, respectively (Fig. 3). We wish to stress that the S computed by considering the core (region where the normalized z component of the magnetization is larger than 0.1) of the radial vortex only is $|S| = 0.5$ and does not depend on $|D|$. The additional contribution to S is due to the IDMI boundary conditions, which lead the magnetization near the sample edges to be tilted out of plane [24].

For $|D| > 2.4$ mJ/m^2, the compensation of the in-plane anisotropy favors the out-of-plane easy axis of the magnetization, and multidomain patterns arise, because the IDMI energy is minimized as the number of Néel DWs

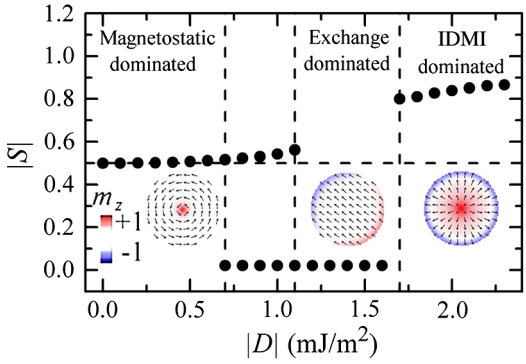

FIG. 3. Skyrmion number as a function of $|D|$. Four different regions are indicated and separated by vertical dashed lines. Insets: examples of spatial distribution of the magnetization related to each region. The colors refer to the z component of the magnetization (blue negative, red positive).

increases. For example, when $|D| = 2.5$ mJ/m^2, a "horseshoelike" domain is obtained, with internal magnetization aligned along the positive z direction, separated from an opposite domain through Néel DWs. When $|D|=3.0$mJ/m^2, a number of Néel DWs are nucleated, leading to a "spiderweblike" domains. The equilibrium states are in agreement with our computations based on energetic arguments.

Figure 2(b) shows the final states (after 500 ns) achieved in the presence of thermal fluctuations at room temperature ($T = 300$ K). By comparing Figs. 2(a) and 2(b), it can be observed how the thermal effects influence the stability. In particular, our results show that the stability for the radial vortex is a remanent state at room temperature in the range $1.8 < |D| < 2.1$ mJ/m^2. Similar results have been achieved for disk diameters from 100 to 350 nm [30] (see Supplemental Material) after the study at 0 K.

Nucleation.—A simple procedure to nucleate a radial vortex is a relaxation process from an out-of-plane saturation state. First, a large external out-of-plane magnetic field of 500 mT is applied to saturate the magnetization. The field is then quasistatically decreased, and, below a field value of about 100 mT up to 0 mT, the IDMI promotes the formation of the radial vortex [30] (see Supplemental Material Video 1 for the nucleation process achieved at $|D| = 2.0$ mJ/m^2). This nucleation procedure is robust to a possible tilting angle of the external field with respect to the out-of-plane direction up to $+/-15$ deg, and to thermal fluctuations at room temperature [30]. Similar results are obtained for IDMI values in the range $1.7 < |D| < 2.3$ mJ/m^2.

Response to in-plane external field.—An in-plane field (H_{ext}) shifts circular and radial vortex differently. Let us consider a field applied along the positive x direction. Figure 4(a) displays the results for the radial vortex ($|D| = 2.0$ mJ/m^2). The external field favors the expansion of the region where the x component of the magnetization is parallel to the external field, thus inducing a shift of the core along the negative x direction [insets of Fig. 4(a)]. An $H_{\text{ext}} = 5.0$ mT yields a uniform magnetic state. Figure 4(b) shows the results for the circular vortex ($|D|=0.0$mJ/m^2).

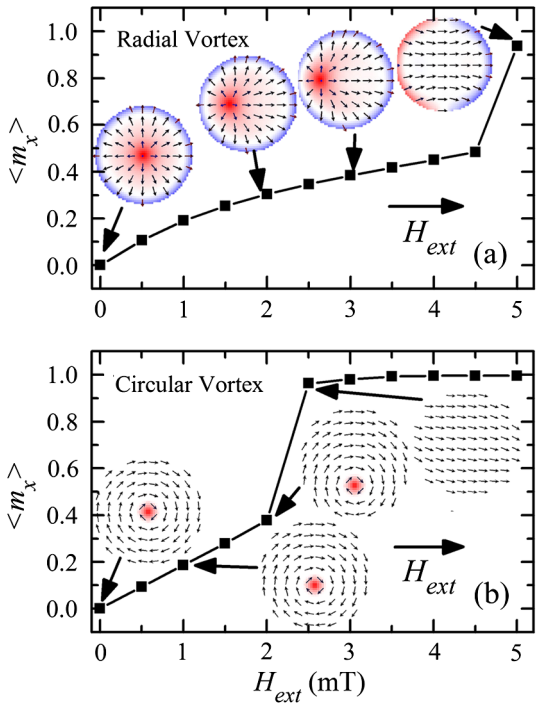

FIG. 4. x component of the normalized magnetization as a function of the external field applied along the positive x direction for (a) the radial vortex, when $|D| = 2.0$ mJ/m^2, and (b) the circular vortex, when $|D| = 0.0$ mJ/m^2. Insets: spatial distributions of the magnetization where the colors indicate the z component (blue negative, red positive). The snapshots for different fields are represented, and the direction of the applied in-plane field is illustrated.

The displacement occurs along the direction perpendicular to the external field [insets Fig. 4(b)] [7,42–45]. Together with the qualitatively different vortex core shift, the field value that leads to the radial vortex core expulsion is twice the one of the circular vortex. This is ascribed to the IDMI and, in particular, to its boundary conditions, in fact, the expulsion field increases as a function of $|D|$. The key reason for that is the need of a larger field to align the out-of-plane tilted spins at the sample edges perpendicular to the vortex core motion. We stress the fact that the different behavior exhibited by the two types of vortices can be considered as a "fingerprint" to detect them in experimental measurements by imaging the vortex core shifting.

Switching.—The second part of this work deals with the switching of radial vortex, implying its possible use in magnetoresistive memories. We focus on the radial vortex at $|D| = 2.0$ mJ/m^2 [24,46–49]. The device is a circularly shaped MTJ, where a CoFeB polarizer is also coupled to a Pt layer. Geometrical and physical parameters of the free layer are the same as the disk described above. The polarizer is designed to have a fixed radial vortex with positive polarity as ground state. A possible strategy to have the polarizer less sensitive to the spin-transfer torque is tailoring the percentage of the Co, Fe, and B to increase the saturation magnetization. A current density J_{MTJ} flows perpendicularly through the whole free layer cross section [30].

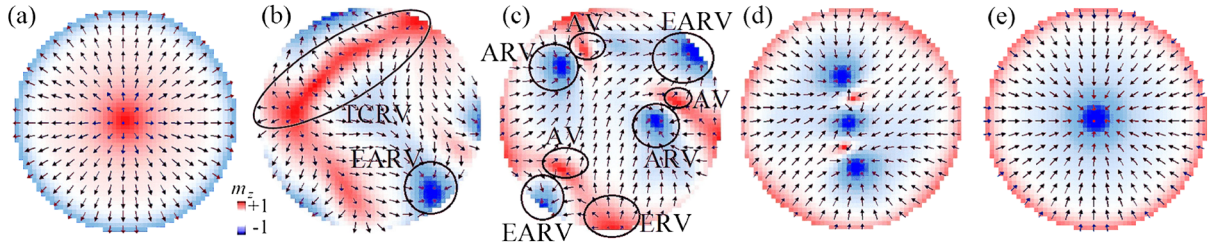

FIG. 5. Example of snapshots for the radial vortex switching at $J_{\mathrm{MTJ}} = 5$ MA/cm^2. (a) Initial state: radial vortex. (b) Topologically connected radial vortices together with an edge antiradial vortex. (c) Three antiradial vortex-antivortex pairs, together with an edge radial and antiradial vortex. (d) Configuration before the accomplishment of the switching: two antiradial vortex-antivortex pairs and one antiradial vortex are clearly observed. (e) Final state: antiradial vortex. The colors are linked to the z component of the magnetization (red positive, blue negative). The acronyms TCRV, ARV, RV, AV, ERV, and EARV indicate the topologically connected radial vortices, antiradial vortex, radial vortex, antivortex, edge radial vortex, and edge antiradial vortex, respectively.

It is possible to identify two switching mechanisms occurring at low ($J_{\mathrm{MTJ}} < 11$ MA/cm^2) and high current densities ($J_{\mathrm{MTJ}} > 11$ MA/cm^2), respectively. We describe the results when the initial state is the radial vortex [snapshot Fig. 5(a)] only, but qualitatively similar mechanisms occur for antiradial → radial switching.

The mechanism at low current density is characterized by a complex process, involving radial and antiradial vortices, antivortices, topologically connected radial vortices, edge radial vortices, and antiradial vortices [50]. It starts with the motion of the radial vortex core towards the boundary of the free layer, accompanied by a core expansion, which gives rise to topologically connected radial vortices, and by a nucleation of an edge antiradial vortex [snapshot Fig. 5(b)]. Afterwards, the topologically connected radial vortices split into two antivortices with positive polarity and an edge radial vortex, while two antiradial vortices and two edge antiradial vortices are nucleated as well [snapshot Fig. 5(c)]. Subsequently, the edge radial vortex annihilates, one antiradial vortex-antivortex pair collapses emitting a spin wave, and the edge antiradial vortex turns into an antiradial vortex. Therefore, before the accomplishment of the switching, a particular magnetization configuration is obtained, composed of two antiradial vortex-antivortex pairs and one antiradial vortex [snapshot Fig. 5(d)]. Finally, the two antiradial vortex-antivortex pairs collapse emitting spin waves, and only the antiradial vortex remains at the center [snapshot Fig. 5(e)] marking the end of the switching [see Supplemental Material Video 2 [30] for the switching process achieved at $J_{\mathrm{MTJ}} = 5$ MA/cm^2].

At high currents (>11 MA/cm^2), the second switching mechanism takes place. The application of the current destroys the radial vortex and promotes the formation of an antiradial vortex together with an antiradial vortex-antivortex pair. Subsequently, the pair collapses and only the antiradial vortex remains, accomplishing the switching (see Supplemental Material Video 3 [30] for the switching process achieved at $J_{\mathrm{MTJ}} = 15$ MA/cm^2).

For the sake of clarity, we have compared the radial and circular vortex ($|D| = 0.0$ mJ/m^2) switching. The first difference is that, for a circular vortex, the switching mechanism is unique. Starting from a ground state (positive polarity and CW chirality), it involves a core polarity reversal followed by a spin-wave excitation, and, afterwards the chirality switching. The final state is then a CCW circular vortex with negative polarity (see Supplemental Material Video 4 [30] for an example of the switching process at $J_{\mathrm{MTJ}} = 5$ MA/cm^2). This switching process is different from previous mechanisms reported in the literature involving edge solitons [50], gyrotropic motion [51], or vortex-antivortex pairs [52].

Figure 6 summarizes the switching time t_s as a function of the current density for the circular and radial vortex. The key result is the achievement of a critical current $J_{\mathrm{MTJ}} = 0.4$ MA/cm^2 for the radial vortex ($T = 0$ K), one order of magnitude lower than the one of the circular vortex ($J_{\mathrm{MTJ}} = 4$ MA/cm^2). However, for $J_{\mathrm{MTJ}} > 4.0$ MA/cm^2, the switching time is shorter for the circular vortex, being its switching mechanism less complex. For the radial vortex, the thermal fluctuations at room temperature ($T = 300$ K) reduce the critical current density to 0.1 MA/cm^2 (Ikeda *et al.* [53] and Amiri *et al.* [54] measured 2 MA/cm^2, whereas Mangin *et al.* 7 MA/cm^2 [55]), while keeping the same value for the circular vortex. Moreover, the radial vortex switching time decreases below the one of the circular

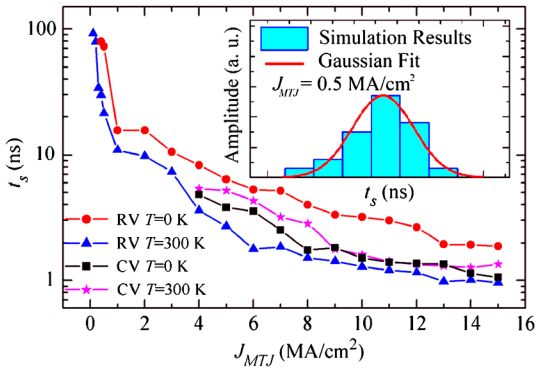

FIG. 6. The main panel shows the switching time as a function of the current density for the radial vortex (RV) and the circular vortex (CV) at $T = 0$ K and $T = 300$ K, as indicated in the legend. Inset: example of histogram related to 100 realizations performed for RV at $T = 300$ K for $J_{\mathrm{MTJ}} = 0.5$ MA/cm^2, and the corresponding Gaussian fit.

vortex, because the thermal fluctuations delete the nucleation of most of the metastable states observed during the radial vortex switching mechanisms at $T = 0$ K. The inset shows an example of the statistical distribution of the switching time for $J_{MTJ} = 0.5$ MA/cm^2, as obtained by performing 100 realizations at $T = 300$ K. We represent the close qualitative agreement between the histogram (cyan bars) and the corresponding Gaussian distribution (red curve) of the data, as built using the mean ($\mu = 23.3$ ns) and standard deviation ($\sigma = 3.5$ ns) of the numerical results.

A final remark is about the effect of the damping on the critical current density: our simulations show a value <0.55 MA/cm^2 at $\alpha = 0.1$.

In summary, we have found that a large enough IDMI lifts the chirality degeneracy of a circular vortex state, promoting the formation of a vortex with a radial chirality. The results have shown that this topological state is robust against thermal fluctuations and can be used for room temperature applications. We have suggested a way for the experimental detection of the radial vortex by the application of an in-plane magnetic field. Besides, the radial vortex switching exhibits very low critical current densities, one order of magnitude lower than the circular vortex state, which are suitable for the development of low power storage devices and nonuniform magnetization state based magnetoresistive memories. Finally, the switching process gives rise to an intrinsic reversal of both polarity and radial chirality of the vortex because of the topological constraint introduced by the IDMI, with the relevant advantage to achieve a full TMR signal change in the characterization of parallel and antiparallel states.

This work was supported by Project No. PRIN2010ECA8P3 from Italian MIUR and by the bilateral agreement Italy-Turkey (TUBITAK-CNR) project (CNR Grant No. B52I14002910005, TUBITAK Grant No. 113F378) "Nanoscale magnetic devices based on the coupling of Spintronics and Spinorbitronics." R. T. acknowledges Fondazione Carit–Projects—"Sistemi Phased-Array Ultrasonori" and "Sensori Spintronici." The simulations were performed in the Scientific Computing Laboratory (SCL) of the University of Messina, Italy.

G. S. and R. T. contributed equally to this work.

*Corresponding author.
gfinocchio@unime.it

[1] M. Kläui, P.-O. Jubert, R. Allenspach, A. Bischof, J. A. C. Bland, G. Faini, U. Rüdiger, C. A. F. Vaz, L. Vila, and C. Vouille, Phys. Rev. Lett. **95**, 026601 (2005).
[2] I. M. Miron, T. Moore, H. Szambolics, L. D. Buda-Prejbeanu, S. Auffret, B. Rodmacq, S. Pizzini, J. Vogel, M. Bonfim, A. Schuhl, and G. Gaudin, Nat. Mater. **10**, 419 (2011).
[3] K.-S. Ryu, L. Thomas, S.-H. Yang, and S. Parkin, Nat. Nanotechnol. **8**, 527 (2013).
[4] S. Emori, U. Bauer, S.-M. Ahn, E. Martinez, and G. S. D. Beach, Nat. Mater. **12**, 611 (2013).
[5] M. R. Pufall, W. H. Rippard, M. L. Schneider, and S. E. Russek, Phys. Rev. B **75**, 140404(R) (2007).
[6] K. Yamada, S. Kasai, Y. Nakatani, K. Kobayashi, H. Kohno, A. Thiaville, and T. Ono, Nat. Mater. **6**, 270 (2007).
[7] V. S. Pribiag, I. N. Krivorotov, G. D. Fuchs, P. M. Braganca, O. Ozatay, J. C. Sankey, D. C. Ralph, and R. A. Buhrman, Nat. Phys. **3**, 498 (2007).
[8] R. Hertel, S. Gliga, M. Fähnle, and C. M. Schneider, Phys. Rev. Lett. **98**, 117201 (2007).
[9] M.-Y. Im, P. Fischer, K. Yamada, T. Sato, S. Kasai, Y. Nakatani, and T. Ono, Nat. Commun. **3**, 983 (2012).
[10] A. Giordano, V. Puliafito, L. Torres, M. Carpentieri, B. Azzerboni, and G. Finocchio, IEEE Trans. Magn. **50**, 4300404 (2014).
[11] V. Sluka, A. Kákay, A. M. Deac, D. E. Bürgler, C. M. Schneider, and R. Hertel, Nat. Commun. **6**, 6409 (2015).
[12] A. Fert, V. Cros, and J. Sampiao, Nat. Nanotechnol. **8**, 152 (2013); J. Sampaio, V. Cros, S. Rohart, A. Thiaville, and A. Fert, Nat. Nanotechnol. **8**, 839 (2013).
[13] R. H. Liu, W. L. Lim, and S. Urazhdin, Phys. Rev. Lett. **114**, 137201 (2015).
[14] Y. Zhou, E. Iacocca, A. A. Awad, R. K. Dumas, F. C. Zhang, H. B. Braun, and J. Åkerman, Nat. Commun. **6**, 8193 (2015); M. Carpentieri, R. Tomasello, R. Zivieri, and G. Finocchio, Sci. Rep. **5**, 16184 (2015).
[15] Y. Zhou and M. Ezawa, Nat. Commun. **5**, 4652 (2014); X. Zhang, M. Ezawa, and Y. Zhou, Sci. Rep. **5**, 9400 (2015).
[16] W. Jiang, P. Upadhyaya, W. Zhang, G. Yu, M. B. Jungfleisch, F. Y. Fradin, J. E. Pearson, Y. Tserkovnyak, K. L. Wang, O. Heinonen, S. G. E. te Velthuis, and A. Hoffmann, Science **349**, 283 (2015).
[17] G. Finocchio, M. Ricci, R. Tomasello, A. Giordano, M. Lanuzza, V. Puliafito, P. Burrascano, B. Azzerboni, and M. Carpentieri, Appl. Phys. Lett. **107**, 262401 (2015).
[18] J. C. Slonczewski, J. Magn. Magn. Mater. **159**, L1 (1996); L. Berger, Phys. Rev. B **54**, 9353 (1996).
[19] R. Tomasello, E. Martinez, R. Zivieri, L. Torres, M. Carpentieri, and G. Finocchio, Sci. Rep. **4**, 6784 (2014).
[20] I. Dzyaloshinskii, J. Phys. Chem. Solids **4**, 241 (1958); T. Moriya, Phys. Rev. Lett. **4**, 228 (1960).
[21] M. Yan, H. Wang, and C. E. Campbell, J. Magn. Magn. Mater. **320**, 1937 (2008).
[22] F. Garcia-Sanchez, J. Sampaio, N. Reyren, V. Cros, and J.-V. Kim, New J. Phys. **18**, 075011 (2016).
[23] X. Dong, X. Weng, H. Guo, and S. Zhuang, Optik (Stuttgart) **123**, 391 (2012).
[24] M. Cubukcu, J. Sampaio, K. Bouzehouane, D. Apalkov, A. V. Khvalkovskiy, V. Cros, and N. Reyren, Phys. Rev. B **93**, 020401(R) (2016).
[25] L. Lopez-Diaz, D. Aurelio, L. Torres, E. Martinez, M. A. Hernandez-Lopez, J. Gomez, O. Alejos, M. Carpentieri, G. Finocchio, and G. Consolo, J. Phys. D **45**, 323001 (2012).
[26] A. Giordano, G. Finocchio, L. Torres, M. Carpentieri, and B. Azzerboni, J. Appl. Phys. **111**, 07D112 (2012).
[27] G. Finocchio, I. N. Krivorotov, X. Cheng, L. Torres, and B. Azzerboni, Phys. Rev. B **83**, 134402 (2011).
[28] R Tomasello, M. Carpentieri, and G. Finocchio, J. Appl. Phys. **115**, 17C730 (2014).
[29] S. Rohart and A. Thiaville, Phys. Rev. B **88**, 184422 (2013).

[30] See Supplemental Material at http://link.aps.org/supplemental/10.1103/PhysRevLett.117.087204, which includes Refs. [31–40], for the details of the micromagnetic model, the parameters used, the stability of the radial vortex in disks with different diameters, and the nucleation process at zero and room temperature.
[31] W. F. Brown, Phys. Rev. **130**, 1677 (1963).
[32] J. C. Slonczewski, Phys. Rev. B **71**, 024411 (2005); J. C. Slonczewski and J. Z. Sun, J. Magn. Magn. Mater. **310**, 169 (2007).
[33] J. C. Sankey, Y.-T. Cui, J. Z. Sun, J. C. Slonczewski, R. A. Buhrman, and D. C. Ralph, Nat. Phys. **4**, 67 (2008).
[34] Z. Zeng, G. Finocchio, B. Zhang, P. K. Amiri, J. A. Katine, I. N. Krivorotov, Y. Huai, J. Langer, B. Azzerboni, K. L. Wang, and H. Jiang, Sci. Rep. **3**, 1426 (2013).
[35] C. Phatak, A. K. Petford-Long, and O. Heinonen, Phys. Rev. Lett. **108**, 067205 (2012).
[36] S. Mühlbauer, B. Binz, F. Jonietz, C. Pfleiderer, A. Rosch, A. Neubauer, R. Georgii, and P. Böni, Science **323**, 915 (2009); X. Z. Yu, Y. Onose, N. Kanazawa, J. H. Park, J. H. Han, Y. Matsui, N. Nagaosa, and Y. Tokura, Nature (London) **465**, 901 (2010).
[37] N. Romming, C. Hanneken, M. Menzel, J. E. Bickel, B. Wolter, K. Von Bergmann, A. Kubetzka, and R. Wiesendanger, Science **341**, 636 (2013); N. Romming, A. Kubetzka, C. Hanneken, K. von Bergmann, and R. Wiesendanger, Phys. Rev. Lett. **114**, 177203 (2015).
[38] J. Iwasaki, M. Mochizuki, and N. Nagaosa, Nat. Commun. **4**, 1463 (2013); J. Iwasaki, M. Mochizuki, and N. Nagaosa, Nat. Nanotechnol. **8**, 742 (2013).
[39] C. Moreau-Luchaire *et al.*, Nat. Nanotechnol. **11**, 444 (2016); O. Boulle *et al.*, Nat. Nanotechnol. **11**, 449 (2016); S. Woo *et al.*, Nat. Mater. **15**, 501 (2016).
[40] F. Ma, M. Ezawa, and Y. Zhou, Sci. Rep. **5**, 15154 (2015).
[41] V. Puliafito, L. Torres, O. Ozatay, T. Hauet, B. Azzerboni, and G. Finocchio, J. Appl. Phys. **115**, 17D139 (2014).
[42] R. P. Cowburn, D. K. Koltsov, A. O. Adeyeye, M. E. Welland, and D. M. Tricker, Phys. Rev. Lett. **83**, 1042 (1999).
[43] K. Y. Guslienko, V. Novosad, Y. Otani, H. Shima, and K. Fukamichi, Appl. Phys. Lett. **78**, 3848 (2001).
[44] A. Neudert, J. McCord, R. Schäfer, and L. Schultz, J. Appl. Phys. **97**, 10E701 (2005).
[45] C. L. Chien, F. Q. Zhu, and J.-G. Zhu, Phys. Today **60**, 40 (2007).
[46] S. Pizzini, J. Vogel, S. Rohart, L. D. Buda-Prejbeanu, E. Jué, O. Boulle, I. M. Miron, C. K. Safeer, S. Auffret, G. Gaudin, and A. Thiaville, Phys. Rev. Lett. **113**, 047203 (2014).
[47] M. Belmeguenai, J.-P. Adam, Y. Roussigné, S. Eimer, T. Devolder, J.-V. Kim, S. M. Cherif, A. Stashkevich, and A. Thiaville, Phys. Rev. B **91**, 180405(R) (2015).
[48] J. Cho, N.-H. Kim, S. Lee, J.-S. Kim, R. Lavrijsen, A. Solignac, Y. Yin, D.-S. Han, N. J. J. van Hoof, H. J. M. Swagten, B. Koopmans, and C.-Y. You, Nat. Commun. **6**, 7635 (2015).
[49] H. Yang, A. Thiaville, S. Rohart, A. Fert, and M. Chshiev, Phys. Rev. Lett. **115**, 267210 (2015).
[50] K.-S. Lee, M.-W. Yoo, Y.-S. Choi, and S.-K. Kim, Phys. Rev. Lett. **106**, 147201 (2011).
[51] K. Y. Guslienko, K.-S. Lee, and S.-K. Kim, Phys. Rev. Lett. **100**, 027203 (2008).
[52] S.-K. Kim, Y.-S. Choi, K.-S. Lee, K. Y. Guslienko, and D.-E. Jeong, Appl. Phys. Lett. **91**, 082506 (2007).
[53] S. Ikeda, K. Miura, H. Yamamoto, K. Mizunuma, H. D. Gan, M. Endo, S. Kanai, J. Hayakawa, F. Matsukura, and H. Ohno, Nat. Mater. **9**, 721 (2010).
[54] P. K. Amiri, Z. M. Zeng, J. Langer, H. Zhao, G. Rowlands, Y.-J. Chen, I. N. Krivorotov, J.-P. Wang, H. W. Jiang, J. A. Katine, Y. Huai, K. Galatsis, and K. L. Wang, Appl. Phys. Lett. **98**, 112507 (2011).
[55] S. Mangin, Y. Henry, D. Ravelosona, J. A. Katine, and E. E. Fullerton, Appl. Phys. Lett. **94**, 012502 (2009).